

JWST/NIRSpec Observations of the Planetary Mass Companion TWA 27B*

K. L. LUHMAN,^{1,2} P. TREMBLIN,³ S. M. BIRKMANN,⁴ E. MANJAVACAS,^{5,6} J. VALENTI,⁷ C. ALVES DE OLIVEIRA,⁸
T. L. BECK,⁷ G. GIARDINO,⁹ N. LÜTZGENDORF,⁴ B. J. RAUSCHER,¹⁰ AND M. SIRIANNI⁴

¹*Department of Astronomy and Astrophysics, The Pennsylvania State University, University Park, PA 16802, USA; kll207@psu.edu*

²*Center for Exoplanets and Habitable Worlds, The Pennsylvania State University, University Park, PA 16802, USA*

³*Université Paris-Saclay, UVSQ, CNRS, CEA, Maison de la Simulation, 91191, Gif-sur-Yvette, France*

⁴*European Space Agency (ESA), ESA Office, Space Telescope Science Institute, 3700 San Martin Drive, Baltimore, MD 21218, USA*

⁵*AURA for the European Space Agency, Space Telescope Science Institute, 3700 San Martin Drive, Baltimore, MD 21218, USA*

⁶*Department of Physics & Astronomy, Johns Hopkins University, Baltimore, MD 21218, USA*

⁷*Space Telescope Science Institute, 3700 San Martin Drive, Baltimore, MD 21218, USA*

⁸*European Space Agency, European Space Astronomy Centre, Camino Bajo del Castillo s/n, 28692 Villanueva de la Cañada, Madrid, Spain*

⁹*ATG Europe for the European Space Agency, ESTEC, Noordwijk, The Netherlands*

¹⁰*NASA Goddard Space Flight Center, Observational Cosmology Laboratory, Greenbelt, USA*

ABSTRACT

We present 1–5 μm spectroscopy of the young planetary mass companion TWA 27B (2M1207B) performed with NIRSpec on board the James Webb Space Telescope. In these data, the fundamental band of CH₄ is absent and the fundamental band of CO is weak. The nondetection of CH₄ reinforces a previously observed trend of weaker CH₄ with younger ages among L dwarfs, which has been attributed to enhanced non-equilibrium chemistry among young objects. The weakness of CO may reflect an additional atmospheric property that varies with age, such as the temperature gradient or cloud thickness. We are able to reproduce the broad shape of the spectrum with an ATM0 cloudless model that has $T_{\text{eff}} = 1300$ K, non-equilibrium chemistry, and a temperature gradient reduction caused by fingering convection. However, the fundamental bands of CH₄ and CO are somewhat stronger in the model. In addition, the model temperature of 1300 K is higher than expected from evolutionary models given the luminosity and age of TWA 27B ($T_{\text{eff}} = 1200$ K). Previous models of young L-type objects suggest that the inclusion of clouds could potentially resolve these issues; it remains to be seen whether cloudy models can provide a good fit to the 1–5 μm data from NIRSpec. TWA 27B exhibits emission in Paschen transitions and the He I triplet at 1.083 μm , which are signatures of accretion that provide the first evidence of a circumstellar disk. We have used the NIRSpec data to estimate the bolometric luminosity of TWA 27B ($\log L/L_{\odot} = -4.466 \pm 0.014$), which implies a mass of 5–6 M_{Jup} according to evolutionary models.

1. INTRODUCTION

With an age of ~ 10 Myr (Barrado y Navascués 2006; Bell et al. 2015), the TW Hya association (TWA) is the youngest known stellar population within 100 pc (de la Reza et al. 1989; Gregorio-Hetem et al. 1992; Kastner et al. 1997; Webb et al. 1999; Gagné et al. 2017; Luhman 2023). Because of its youth and proximity, Gizis (2002) performed a survey for brown dwarfs in TWA using photometry from the Two Micron All Sky Survey shortly after its completion (2MASS,

Skrutskie et al. 2006). Two substellar members of TWA were discovered through that work, 2MASSW J113951–3159211 and 2MASSW J1207334–393254, which were later assigned the designations of TWA 26 and 27, respectively (Mamajek 2005). During a survey for substellar companions with adaptive optics imaging, Chauvin et al. (2004) discovered a faint candidate with a projected separation of $0''.78$ from TWA 27. They verified its cool nature through near-infrared (IR) spectroscopy and estimated a mass of $\sim 5 M_{\text{Jup}}$ from photometry, which would make it the first directly imaged planetary mass companion outside of the solar system. Companionship was confirmed through additional epochs of imaging that demonstrated a common proper motion with the primary (Chauvin et al. 2005;

* Based on observations made with the NASA/ESA/CSA James Webb Space Telescope, the Gaia mission, the Two Micron All Sky Survey, and the Wide-field Infrared Survey Explorer.

Song et al. 2006). Although the secondary is well within the mass range of extrasolar planets (Howard et al. 2010), it likely formed in the manner of a binary star rather than as a planet in a circumstellar disk given the large mass ratio of the pair (~ 0.2) compared to the typical value of $M_{\text{disk}}/M_{\text{star}}$ for low-mass stars and brown dwarfs (~ 0.01 , Andrews et al. 2013; Mohanty et al. 2013), as discussed in Lodato et al. (2005). The mass ratio of the TWA 27 system is also well above the upper limit of ~ 0.04 in the International Astronomical Union’s working definition of an exoplanet (Lecavelier des Etangs & Lissauer 2022).

Since its discovery, TWA 27B has been the subject of numerous studies to characterize its stellar and atmospheric properties. One parameter that is important in such analysis is the distance, which has been estimated for the primary using the moving cluster method (Mamajek 2005; Mamajek & Meyer 2007) and parallax (Biller & Close 2007; Gizis et al. 2007; Ducourant et al. 2008). Currently, the most accurate distance for TWA 27A is 64.5 ± 0.4 pc (Bailer-Jones et al. 2021), which is based on a parallax measurement from the third data release of the Gaia mission (Gaia Collaboration et al. 2016, 2021, 2022).

For all of the distances previously adopted for TWA 27B, which have ranged from ~ 53 – 70 pc, the luminosity derived from its near-IR photometry and a bolometric correction for field dwarfs has been much lower than predicted for an object at the age of TWA and at the effective temperature implied by both model fits to its spectrum (Mohanty et al. 2007; Patience et al. 2012) and the combination of its spectral type (mid-to-late L, Chauvin et al. 2004; Mohanty et al. 2007; Patience et al. 2010; Allers & Liu 2013) and the temperature scale for field dwarfs (Golimowski et al. 2004). Initial attempts were made to explain this seemingly anomalous property (Mamajek & Meyer 2007; Mohanty et al. 2007). However, the discovery of additional young L/T dwarfs and planets has demonstrated that TWA 27B is not unusual for its mass and age (Metchev & Hillenbrand 2006; Luhman et al. 2007; Metchev et al. 2009; Bowler et al. 2010; Currie et al. 2011; Skemer et al. 2011, 2014; Faherty et al. 2012, 2016; Liu et al. 2013, 2016; Filippazzo et al. 2015). The discrepancies between the inferred temperatures and luminosities of young late-type objects like TWA 27B and the values predicted by evolutionary models likely reflect age dependencies of the temperature scale and the near-IR bolometric corrections. Namely, at younger ages, a given spectral type corresponds to a cooler temperature and a smaller fraction of the flux is emitted at near-IR wavelengths. The spectral energy distributions (SEDs)

of young late-type objects have been broadly reproduced by models of cloudy, low-gravity atmospheres that experience non-equilibrium chemistry (Barman et al. 2011a,b; Madhusudhan et al. 2011; Marley et al. 2012; Skemer et al. 2011, 2014; Charnay et al. 2018) as well as models of cloudless atmospheres that have a temperature gradient reduction caused by fingering convection (Tremblin et al. 2017).

TWA 27B continues to play an important role in understanding the early evolution of planetary mass objects because of its well-determined distance and age and the paucity of known objects with a similar combination of age and mass. In this paper, we seek to use the Near-Infrared Spectrograph (NIRSpec, Jakobsen et al. 2022) on board the James Webb Space Telescope (JWST, Gardner et al. 2023) to measure the SED of TWA 27B more accurately and across a wider range of wavelengths than done in previous studies.

2. OBSERVATIONS

The TWA 27 system was observed with NIRSpec’s integral-field unit (IFU, Böker et al. 2022) through guaranteed time observation program 1270 (PI: S. Birkmann) on 2023 February 7 (UT). The IFU has a large enough field of view ($3''.1 \times 3''.2$) that it was able to observe both components of the system at the same time. Data were collected with the following grating/filter combinations, which provided a spectral resolution of ~ 2700 : G140H/F100LP (0.97 – $1.89 \mu\text{m}$), G235H/F170LP (1.66 – $3.17 \mu\text{m}$), and G395H/F290LP (2.87 – $5.27 \mu\text{m}$). The resulting data have gaps at 1.42 – 1.47 , 2.39 – 2.47 , and 4.03 – $4.17 \mu\text{m}$ from the physical separation between the two detector arrays. For each configuration, we used either 31 or 32 groups, four dithers, and the NRSIRS2RAPID readout pattern, resulting in a total exposure time of ~ 1900 s. To facilitate the subtraction of TWA 27A when extracting the spectrum of its companion, identical observations were performed for TWA 28 (SSSPMJ1102–3431, Scholz et al. 2005a), which has a similar spectral type and brightness as TWA 27A. The position angle of the telescope was selected to avoid bright stars falling within the field of view of the microshutter assembly.

3. DATA REDUCTION

We have reduced the NIRSpec data for the TWA sources as well as similar observations of the planetary mass companion VHS J125601.92–125723.9b (VHS 1256b, Gauza et al. 2015) from program 1386 (Hinkley et al. 2022), which were first reported by Miles et al. (2023). It is useful to compare the spectra of TWA 27B and VHS 1256b since they have roughly similar spectral types but different ages.

For the data reduction, we began by retrieving the `uncal` files from the Mikulski Archive for Space Telescopes (MAST): [doi:10.17909/jzze-5611](https://doi.org/10.17909/jzze-5611). We performed ramps-to-slopes processing on those files using the NIRSpec Instrument Pipeline Software¹, which features a correction for “snowballs” (Böker et al. 2023) and a correction for residual correlated noise in IFU data. The resulting count rate maps (`rate` files) were used as inputs to the JWST `calwebb_spec2` pipeline with the default processing steps, including assignment of the World Coordinate System, flat fielding, and aperture correction. We used the JWST Science Calibration pipeline version 1.9.4 under Calibration Reference Data System context `jwst_1063.pmap`. We flagged outliers in the resulting `cal` files and then constructed the IFU data cubes using the `calwebb_spec3` pipeline with outlier detection disabled. The latter was necessary as currently the pipeline’s outlier detection is not working properly, resulting in many erroneously flagged data points and poor final cubes. We selected a spaxel size of $0''.1$ for the cubes and used the “ifualign” coordinate system to provide the same point spread function (PSF) orientation among observations of different targets. Spectra for TWA 27A, TWA 28, and VHS 1256b were extracted from these cubes with an aperture radius of 4 spaxels. Before extracting TWA 27B, PSF subtraction was applied to the primary using a version of the data cube for TWA 28 that had been scaled and shifted appropriately. In Figure 1, we show the 2-D images of TWA 27A and B for each of the three gratings before and after PSF subtraction. Flux calibration was performed with observation 62 for standard star P330E from program 1538 (PI: Karl Gordon), which utilized the NIRpec IFU with the same gratings and filters as our observations. The reduced spectra of TWA 27B and VHS 1256b are available at [doi:10.5281/zenodo.7876159](https://doi.org/10.5281/zenodo.7876159).

We have compared the reduced spectra of VHS 1256b from this work and Miles et al. (2023). For some wavelength ranges, our version of the spectrum has less low-order structure and exhibits a more smoothly varying continuum. For instance, the absorption feature near $1.66\ \mu\text{m}$ that was noted by Miles et al. (2023) is absent from our reduction.

We have derived synthetic photometry from our reduced spectra of the TWA sources and VHS 1256b, which we use to assess the accuracy of the absolute fluxes in these data. Such measurements also facilitate comparisons to other late-type objects (Section 4.2). We have selected the following bands for

synthetic photometry: JHK_s from 2MASS, JHK from the Mauna Kea Observatories (MKO) system (Tokunaga et al. 2002), the W1 and W2 bands (3.4 and $4.6\ \mu\text{m}$) for the Wide-field Infrared Survey Explorer (WISE, Wright et al. 2010) and the reactivated mission (NEOWISE, Mainzer et al. 2014), and most of the medium- and wide-band filters for NIRCcam on JWST (Rieke et al. 2005, 2023). 2MASS, MKO, and WISE are the most frequently measured filters for substellar objects while the NIRCcam photometry may be useful for comparison to data from that camera in future studies. When calculating the photometry, we interpolated across the three gaps in the spectra.

For comparison to our synthetic photometry, we have considered JHK_s data for TWA 27A and TWA 28 from the 2MASS Point Source Catalog (Skrutskie et al. 2003), JHK data for VHS 1256b from the sixth data release of the Visible and Infrared Survey Telescope for Astronomy (VISTA) Hemisphere Survey (McMahon et al. 2013), and the mean $4.5\ \mu\text{m}$ photometry for VHS 1256b from Zhou et al. (2020) after conversion to W2 (Kirkpatrick et al. 2021). The mean photometry from Zhou et al. (2020) was based on continuous measurements during a 36 hr period. WISE and NEOWISE have provided photometry in W1 and W2 for TWA 27A and TWA 28 at multiple epochs between 2010 and 2022. The data are clustered in epochs that span 1–4 days, each containing 11–31 single exposures. TWA 27A and TWA 28 were observed at 21 and 20 epochs, respectively. For each epoch and band, we have calculated the median and standard deviation of the single-exposure measurements from the AllWISE Multiepoch Photometry Table (Wright et al. 2013) and the NEOWISE-R Single Exposure Source Table (Cutri et al. 2023). The resulting measurements are plotted versus time in Figure 2. For individual epochs, the standard deviations are typically 0.02–0.04 mag, which serve as upper limits on the variability on timescales of hours. For each object and band, the standard deviation of the medians across all epochs is $\lesssim 0.02$ mag. The medians of the medians across all epochs are $W1=11.58$ and $W2=11.03$ for TWA 27A and $W1=11.46$ and $W2=10.83$ for TWA 28, which are adopted for comparison to the NIRSpec photometry.

The differences between the synthetic photometry from NIRSpec and the photometry from previous measurements, $m_{\text{NIRSpec}} - m_{\text{phot}}$, are 0.05 (J), 0.04 (H), 0.06 (K_s), -0.03 ($W1$), and 0.00 ($W2$) for TWA 27A, 0.02 (J), 0.03 (H), 0.04 (K_s), -0.07 ($W1$), and -0.04 ($W2$) for TWA 28, and 0.09 (J), -0.11 (H), -0.05 (K), and 0.05 ($W2$) for VHS 1256b. These results do not show a systematic offset across all bands and objects, indicat-

¹ <https://jwst-tools.cosmos.esa.int/index.html>

ing that the flux calibrations of the spectra are fairly accurate. The differences in photometry can be plausibly explained by variability. In particular, the wide range of offsets for VHS 1256b is not surprising given that it is known to exhibit large wavelength-dependent variability (Bowler et al. 2020; Zhou et al. 2020, 2022a). The synthetic photometry in Vega magnitudes from the NIRSpec data is presented in Table 1. The photometric errors should be dominated by the uncertainty in the flux calibration for the NIRSpec data, for which we have adopted a value of 3%.

4. ANALYSIS

4.1. Comparison to Previous Spectroscopy

Extensive spectroscopy has been performed on TWA 27A and TWA 28 from UV through mid-IR wavelengths (Gizis 2002; Scholz et al. 2005b; Looper et al. 2007; Morrow et al. 2008; Herczeg et al. 2009; Rice et al. 2010; Bonnefoy et al. 2014; Herczeg & Hillenbrand 2014; Venuti et al. 2019) while more limited spectra have been collected at 1–2.5 μm for TWA 27B (Chauvin et al. 2004; Mohanty et al. 2007; Patience et al. 2010). To compare the broad near-IR spectral shapes measured by NIRSpec and other spectrographs, we show in Figure 3 the NIRSpec data and low-resolution spectra from SpeX (Rayner et al. 2003) at the NASA Infrared Telescope Facility for TWA 27A and TWA 28 (Looper et al. 2007; Luhman et al. 2017) and a spectrum from SINFONI (Eisenhauer et al. 2003) on the Very Large Telescope for TWA 27B (Patience et al. 2010). The NIRSpec and SINFONI spectra have been binned to a resolution of $R=200$. The NIRSpec and SpeX data agree very closely. The SINFONI spectrum for TWA 27B is significantly redder than the NIRSpec data from 1.2–1.7 μm , which is likely caused by the large uncertainties in the J and K photometric measurements (Chauvin et al. 2004; Mohanty et al. 2007) that were used to determine the relative flux calibration of the J and HK spectra from SINFONI. Meanwhile, the NIRSpec data are somewhat redder than the SINFONI spectrum at 1.7–2.4 μm . TWA 27B had $J - K = 3.07 \pm 0.23$ based on the photometry from Chauvin et al. (2004) and Mohanty et al. (2007), which has made it one of the reddest known L-type objects. However, we derive $J - K = 2.72$ (MKO) from the NIRSpec data, indicating that TWA 27B is not quite as red as previously reported.

4.2. Comparison to Young Late-type Objects

The photometric properties of young late-type objects can be examined with IR color-color and color-magnitude diagrams (CMDs). In Figure 4, we have

plotted TWA 27B on diagrams of $K - W2$ and M_K versus $J - K$ using the synthetic photometry measured with NIRSpec. The J and K data are on the MKO system. For comparison, we have included the sample of L-type dwarfs and planetary mass companions with $J - K > 2.2$ compiled by Schneider et al. (2023) (most have ages of $\lesssim 200$ Myr) and the known members of Upper Sco ($\gtrsim M9$, Luhman & Esplin 2022, K. Luhman, in preparation) that are located within the central triangular field of the association defined by Luhman & Esplin (2020). Upper Sco offers the largest available sample of planetary mass brown dwarfs near the age of TWA. When calculating M_K for Upper Sco members, we have used the parallactic distances from Bailer-Jones et al. (2021) when available and otherwise have adopted the median distance of 144 pc for the members of Upper Sco within the field in question. Among the L-type objects compiled by Schneider et al. (2023), some of the free-floating dwarfs lack parallax measurements (absent from the CMD) and some of the companions lack photometry in $W2$ (absent from $K - W2$ versus $J - K$).

Most of the objects in Figure 4 form a fairly well-defined locus in each diagram. In the CMD, the locus begins to turn back to bluer colors with the faintest object, HD 8799b, which is the behavior observed in the transition from L to T types among normal field dwarfs (Burgasser et al. 2002). The red outlier in $J - K$ is HD 206893B (Milli et al. 2017). TWA 27B appears along the red edge of the locus and is less extreme in $J - K$ using our photometry than in previous studies, as mentioned in Section 4.1. The data in Figure 4 illustrate that TWA 27B is not anomalous relative to other young planetary mass objects, which has become widely recognized over the last decade.

In Figure 5, we compare the near-IR spectrum of TWA 27B to data for two of the reddest L dwarfs from Figure 4, CWISE J050626.96+073842.4 (CWISE 0506, Schneider et al. 2023) and PSO J318.5338–22.8603 (POS 318, Liu et al. 2013). We also include our reduction of the NIRSpec observations of VHS 1256b since it is the only object from Figure 4 other than TWA 27B that has NIRSpec data available. Since we are comparing their broad shapes, the spectra have been binned to a resolution of $R=200$. TWA 27B is bluer than CWISE 0506 and slightly redder than PSO 318 and VHS 1256b, which is consistent with their $J - K$ colors. The shapes of the H - and K -band continua differ somewhat between TWA 27B and the other objects, which is likely because of older ages for the latter. Both PSO 318 and CWISE 0506 have been classified as likely members of the β Pic association (Allers et al. 2016; Schneider et al. 2023), which has an age of ~ 21 –24 Myr (Binks & Jeffries

2016), while an age of 140 ± 20 Myr has been estimated for the VHS 1256 system (Dupuy et al. 2023)

Spectroscopy has not been performed previously on TWA 27B longward of the K band. In Figure 6, we show its 2.5–5.3 μm spectrum from NIRSpec with the NIRSpec data for VHS 1256b and a 3–4 μm ground-based spectrum of PSO 318 (Beiler et al. 2023) (see also Miles et al. (2018)). CWISE 0506 has not been observed spectroscopically at these wavelengths. Although TWA 27B and VHS 1256b have roughly similar near-IR spectra, their 3–5 μm spectra exhibit notable differences. VHS 1256b has strong absorption in the Q -branch of the ν_3 fundamental band of CH_4 at 3.33 μm , broader shallow absorption in the surrounding P - and R -branches, and strong absorption from the fundamental band of CO at 4.4–5.2 μm , as discussed by Miles et al. (2023) in their analysis of the NIRSpec data. In TWA 27B, CH_4 absorption is not detected and the CO lines are much weaker. The CH_4 absorption in PSO 318 appears to be similar to or slightly weaker than that of VHS 1256b. The origins of these differences in CH_4 and CO are discussed in the next section.

4.3. Comparison to Model Spectra

As mentioned in Section 1, it has been possible to identify both cloudy and cloudless models that can reproduce the general shapes of the SEDs of young L-type objects. In the case of TWA 27B, modeling has been applied to the near-IR spectra from Patience et al. (2010) and Mohanty et al. (2007) and the 3–4 μm photometry from Chauvin et al. (2004) and Skemer et al. (2014) (Mohanty et al. 2007; Barman et al. 2011b; Skemer et al. 2011, 2014; Patience et al. 2010, 2012). In this study, we have attempted to fit the 1–5 μm data for TWA 27B from NIRSpec with spectra predicted by the ATMO models of cloudless brown dwarfs (Tremblin et al. 2015, 2017). In these models, diabatic convective processes (Tremblin et al. 2019) induced by non-equilibrium chemistry of CO/ CH_4 and N_2/NH_3 reduce the temperature gradient in an atmosphere and reproduce the red near-IR colors of L dwarfs (Tremblin et al. 2016). Petrus et al. (2023) described a recent grid of the models in which the parameters were effective temperature (T_{eff}), surface gravity ($\log g$), effective adiabatic index (γ), eddy diffusion coefficient (K_{zz}), metallicity ($[\text{M}/\text{H}]$), and C/O ratio. We utilized that model grid for an initial fit to the NIRSpec data for TWA 27B and we calculated additional models to further refine the fit, converging on a model with $T_{\text{eff}} = 1300$ K, $\log g = 3.5$, $\gamma = 1.03$, $K_{\text{zz}} = 10^5$, $[\text{M}/\text{H}] = 0.2$, and a solar value for C/O. The absolute

fluxes of the NIRSpec data lead to a radius of $0.116 R_{\odot}$ for that model.

In Figure 7, we show the NIRSpec and model spectra after binning both to a resolution of $R=200$. The model agrees quite well with the data overall. The primary differences consist of the shapes of the H - and K -band continua, the flux at 3–4 μm , and the strengths of CH_4 at 3.33 μm and CO at 4.4–5.2 μm , where both of the latter features are stronger in the model. The inclusion of clouds could potentially improve the fit since they should reduce the strengths of those features (Barman et al. 2011b). The temperature and radius of the model for TWA 27B correspond to an age of ~ 100 Myr according to evolutionary models (Chabrier et al. 2023), which is much older than the age of ~ 10 Myr implied by a comparison of the primary to evolutionary models and various age constraints for the association (e.g., Luhman 2023). This discrepancy likely reflects remaining deficiencies in the adopted atmospheric model such that the true temperature and radius of TWA 27B are lower and higher, respectively, than the values implied by our SED fitting. For instance, if we assume an age of 10 Myr, our estimate of the luminosity of TWA 27B in Section 4.5 implies a temperature of 1200 K according to evolutionary models, whereas 1300 K was derived from our model fit to the NIRSpec data. Early modeling of TWA 27B’s SED exhibited a larger discrepancy of this kind ($T_{\text{eff}} \sim 1600$ K, Mohanty et al. 2007; Patience et al. 2010) while models that included non-equilibrium chemistry and thick clouds produced lower temperatures that were less discrepant ($T_{\text{eff}} \sim 1000$ K, Barman et al. 2011b).

Miles et al. (2018, 2023) found that the 3.33 μm CH_4 band is weaker in VHS 1256b than in field L dwarfs, which they attributed to non-equilibrium chemistry in VHS 1256b. Weak CH_4 also has been observed in other young L dwarfs with ages of ~ 10 –100 Myr (Beiler et al. 2023). That trend of weaker CH_4 with younger age continues with TWA 27B, where the feature is absent. In addition to weakening CH_4 , an enhancement of non-equilibrium chemistry should strengthen the fundamental band of CO (Skemer et al. 2014; Mukherjee et al. 2022), so the fact that both CH_4 and CO are significantly weaker in TWA 27B than in VHS 1256b indicates the influence of an additional atmospheric property that varies with age, such as the temperature gradient (Tremblin et al. 2015, 2017) or cloud thickness (Barman et al. 2011b; Skemer et al. 2014; Charnay et al. 2018).

4.4. Evidence of Circumstellar Disks

Spectra like those collected with NIRSpec in TWA can contain signatures of circumstellar disks in the form of emission lines or mid-IR emission in excess above that expected from a stellar photosphere. TWA 27A and TWA 28 have previous evidence of disks from some combination of UV emission lines and continuum (Gizis et al. 2005; Herczeg et al. 2009; France et al. 2010; Venuti et al. 2019), H α emission (Mohanty et al. 2003; Scholz et al. 2005b; Stelzer et al. 2007), mid- and far-IR excess emission (Sterzik et al. 2004; Riaz et al. 2006; Riaz & Gizis 2008; Morrow et al. 2008; Harvey et al. 2012), and millimeter emission (Mohanty et al. 2013; Ricci et al. 2017). An outflow also has been detected from TWA 27A (Whelan et al. 2007, 2012). The near-to-mid-IR colors derived from the NIRSpec data for TWA 27A and TWA 28 (e.g., $J-W1$ and $J-W2$) are similar to colors from 2MASS, WISE, and the Spitzer Space Telescope, and thus exhibit color excesses from disks that are consistent with those measured in previous studies (Riaz et al. 2006; Schneider et al. 2012).

Given its faintness and small separation from the primary, TWA 27B has had few constraints on the presence of a disk. Ricci et al. (2017) performed sensitive observations with the Atacama Large Millimeter Array (ALMA) that were capable of resolving the components of TWA 27, but no emission was detected from the secondary. They derived a 3σ upper limit of $\sim 0.013 M_{\oplus}$ ($\sim 1 M_{\text{Moon}}$) on the mass of dust surrounding TWA 27B. By extending longward of previous IR measurements, the NIRSpec data at 4–5 μm provide a new constraint on disk emission. Our synthetic NIRSpec photometry in the W2 band spans that wavelength range. The color-color diagram in Figure 4 shows that TWA 27B does not exhibit a color excess in $K-W2$ relative to other young objects with similar values of $J-K$, which indicates that it lacks excess emission in W2.

Although the available mid-IR and millimeter data for TWA 27B have not detected disk emission, the NIRSpec spectrum does contain detections of emission in Paschen transitions (α , β , γ , and possibly δ) and the (blended) He I triplet at 1.083 μm , as shown in Figure 8. These emission lines are signatures of accretion when observed in young stars (Natta et al. 2004; Edwards et al. 2006). Estimating an accretion rate from the strength of the He I emission is not straightforward because it is affected by both accretion and winds (Edwards et al. 2006; Erkal et al. 2022; Thanathibodee et al. 2022). Relations between Pa β line luminosity and accretion luminosity are available for stars and brown dwarfs (Natta et al. 2004; Alcalá et al. 2017). It is unknown whether such relations are applicable to brown dwarfs as small in mass

as TWA 27B, but we have used them to derive an accretion luminosity from its Pa β line flux ($6.6 \pm 1.2 \times 10^{-17}$ erg cm $^{-2}$ s $^{-1}$) and the distance of TWA 27A. We have converted the accretion luminosity to an accretion rate in the manner done in Gullbring et al. (1998) by assuming a mass of $0.005 M_{\odot}$ and a radius of $0.14 R_{\odot}$ for TWA 27B, which are expected from evolutionary models for the luminosity and age of the object (Section 4.5). The resulting accretion rate ranges from $\dot{M} \sim 10^{-13}$ – $10^{-12} M_{\odot}$ yr $^{-1}$, which appears to be plausible when extrapolating the relationship between stellar mass and accretion rate for young stars and brown dwarfs to the mass of TWA 27B (Muzerolle et al. 2005; Herczeg & Hillenbrand 2008; Hartmann et al. 2016). Given the dust mass upper limit from ALMA and a standard gas-to-dust ratio of ~ 100 , a disk around TWA 27B could undergo accretion at these rates for $\lesssim 4$ – 40 Myr, which is comparable to the age of TWA. Thus, steady accretion at the rate implied by Pa β appears plausible given the mass constraints from ALMA. If TWA 27B does have a disk, it likely exhibits excess emission in unpublished 5–28 μm data that were obtained with the Mid-infrared Instrument on JWST (MIRI, Rieke et al. 2015) during the same visit as the NIRSpec observations.

TWA 27B joins a small but growing sample of young planetary mass companions in which possible evidence of accretion has been detected via emission lines (Bowler et al. 2011; Lachapelle et al. 2015; Wagner et al. 2018; Haffert et al. 2019; Eriksson et al. 2020; Chinchilla et al. 2021; Currie et al. 2022; Betti et al. 2022; Zhou et al. 2014, 2021, 2022b; Ringqvist et al. 2023). As an aside, we note that one of those companions, 2MASS J01033563–5515561 C (Delorme et al. 2013), appears to lack a spectral classification but does have optical spectroscopy available (Eriksson et al. 2020). We have measured a spectral type of L0 \pm 0.5 from those data based on a comparison to young L-type standards (Cruz et al. 2009, 2018).

4.5. Luminosity and Mass Estimates for TWA 27B

Previous studies have estimated the luminosity of TWA 27B by combining a near-IR band (typically K) with a bolometric correction for L dwarfs and an adopted distance. They then derived a mass by comparing the luminosity to the values predicted by evolutionary models for the age of TWA (Chauvin et al. 2004; Mamajek 2005; Mamajek & Meyer 2007; Ducourant et al. 2008; Barman et al. 2011b). The resulting mass estimates have spanned from ~ 3 – $7 M_{\text{Jup}}$. Since the NIRSpec data have measured the SED of TWA 27B across a wide range

of wavelengths and the primary has a precise distance measurement from Gaia, we can improve the estimates of the luminosity and mass. We have calculated the luminosity of TWA 27B by integrating the flux in the NIRSpec spectrum (1–5.3 μm) and the best fitting model spectra at shorter and longer wavelengths and applying the distance from Bailer-Jones et al. (2021), arriving at $\log L/L_\odot = -4.466 \pm 0.014$. We have adopted the distance error from Bailer-Jones et al. (2021) and a 3% uncertainty in the flux calibration of the NIRSpec data. Our luminosity estimate is similar to those from previous studies after accounting for the differences in adopted distances.

For TWA 27B, we have adopted an age of 10 ± 2 Myr that has been estimated for its association (Luhman 2023). In Figure 9, we have plotted TWA 27B with the luminosities predicted as a function of age for masses of 0.002–0.01 M_\odot by the evolutionary models of Chabrier et al. (2023) and Burrows et al. (1997). Both sets of models imply a mass of 0.005–0.006 M_\odot (5–6 M_{Jup}) for TWA 27B. For an age of 10 Myr, our luminosity estimate corresponds to a temperature of 1200 K according to the evolutionary models, which is lower than the value of 1300 K derived from our model fitting of the SED, as mentioned in Section 4.3.

5. CONCLUSIONS

We have used NIRSpec on JWST to perform 1–5 μm spectroscopy on the young planetary mass companion TWA 27B. We also have reduced similar data for VHS 1256b (Miles et al. 2023), which has a roughly similar spectral type to TWA 27B but an older age (~ 140 Myr). Our results are summarized as follows:

1. We have calculated synthetic photometry from the NIRSpec spectra for TWA 27A, TWA 27B, TWA 28, and VHS 1256b in a variety of bands between 1–5 μm . Given the large errors and limited wavelength range of its previous photometry, the new measurements for TWA 27B are particularly useful for comparison to other young planetary mass objects. We find that TWA 27B is not as red in $J - K$ as reported in previous studies, making it less extreme in that color relative to other young L dwarfs. In diagrams of $K - W2$ and M_K versus $J - K$, it falls within the sequence formed by young L-type dwarfs and planets.
2. NIRSpec has provided the first spectroscopy of TWA 27B at 2.5–5 μm . In these data, the fundamental band of CH_4 is absent and the fundamental band of CO is weak, whereas both features are stronger in VHS 1256b. The nondetec-

tion of CH_4 reinforces a previously observed trend of weaker CH_4 with younger ages among L dwarfs (Miles et al. 2018, 2023; Beiler et al. 2023), which has been attributed to enhanced non-equilibrium chemistry among young objects. Explaining the weak CO in TWA 27B requires that an additional atmospheric property varies with age, such as the temperature gradient or cloud thickness.

3. We have compared the NIRSpec data for TWA 27B to spectra predicted by the ATM0 models of cloudless brown dwarfs (Tremblin et al. 2015, 2017), which include non-equilibrium chemistry and a temperature gradient reduction caused by fingering convection. The broad shape of the spectrum is matched well with a model that has $T_{\text{eff}} = 1300$ K and a low surface gravity. One of the primary differences between the model and observed spectra lies in the fundamental bands of CH_4 and CO, which are somewhat stronger in the model spectrum. Meanwhile, the model temperature of 1300 K is higher than expected from evolutionary models given the luminosity and age of TWA 27B ($T_{\text{eff}} = 1200$ K). Based on previous modeling of young L-type objects like TWA 27B, the inclusion of thick clouds could potentially resolve both issues (e.g., Barman et al. 2011b). It remains to be seen whether cloudy models can provide a good fit to the 1–5 μm data from NIRSpec.
4. NIRSpec has detected emission in three (and perhaps four) Paschen transitions and the He I triplet at 1.083 μm from TWA 27B, which are signatures of accretion when observed in young stars. These emission lines are the first evidence of a circumstellar disk around TWA 27B. Using relations between $\text{Pa}\beta$ line luminosity and accretion luminosity from previous studies of stars and brown dwarfs (Natta et al. 2004; Alcalá et al. 2017), we have estimated an accretion rate of $\dot{M} \sim 10^{-13} - 10^{-12} M_\odot \text{ yr}^{-1}$, which would be roughly consistent with the correlation between stellar mass and accretion rate for young stars and brown dwarfs (Muzerolle et al. 2005; Herczeg & Hillenbrand 2008; Hartmann et al. 2016). TWA 27B does not exhibit excess emission in W2 (4.6 μm) relative to other young L-type objects. If it does have a disk, excess emission is likely present at longer IR wavelengths, which should be detectable with 5–28 μm data from JWST/MIRI that were collected during the same visit as the NIRSpec observations.
5. We have calculated the bolometric luminosity of TWA 27B by integrating its NIRSpec spectrum

and estimating the missing flux at shorter and longer wavelengths with model spectra, arriving at a value of $\log L/L_{\odot} = -4.466 \pm 0.014$. Based on that luminosity and the age its association (10 ± 2 Myr), TWA 27B should have a mass of $5\text{--}6 M_{\text{Jup}}$ according to evolutionary models (Burrows et al. 1997; Chabrier et al. 2023). These luminosity and mass estimates are similar to the values from previous studies.

P.T. acknowledges support from the European Research Council under grant agreement ATMO 757858. The JWST data were obtained from MAST at the Space Telescope Science Institute, which is operated by the Association of Universities for Research in Astronomy, Inc., under NASA contract NAS 5-03127. The JWST observations are associated with programs 1270 and 1386. We acknowledge the team for program 1386 (PI: S. Hinkley) for developing their observing program with a zero-exclusive-access period. This work used data from the ESA mission Gaia (<https://www.cosmos.esa.int/gaia>), processed by the Gaia Data Processing and Analysis Consortium (DPAC, <https://www.cosmos.esa.int/web/gaia/dpac/consortium>). Funding for the DPAC has been provided by national institutions, in particular the institutions participating in the Gaia Multilateral Agreement. 2MASS is a joint project of the University of Massachusetts and IPAC at Caltech, funded by NASA and the NSF. WISE is a joint project of the University of California, Los Angeles, and the JPL/Caltech, funded by NASA. NEOWISE is a joint project of JPL/Caltech and the University of Arizona, funded by NASA. This work used data from the NASA/IPAC Infrared Science Archive, operated by JPL under contract with NASA, and the VizieR catalog access tool and the SIMBAD database, both operated at CDS, Strasbourg, France. The Center for Exoplanets and Habitable Worlds is supported by the Pennsylvania State University, the Eberly College of Science, and the Pennsylvania Space Grant Consortium.

REFERENCES

- Alcalá, J. M., Manara, C. F., Natta, A., et al. 2017, *A&A*, 600, A20
- Allers, K. M., Gallimore, J. F., Liu, M. C., & Dupuy, T. J. 2016, *ApJ*, 819, 133
- Allers, K. N., & Liu, M. C. 2013, *ApJ*, 772, 79
- Andrews, S. M., Rosenfeld, K. A., Kraus, A. L., & Wilner, D. J. 2013, *ApJ*, 771, 129
- Bailer-Jones, C. A. L., Rybizki, J., Fouesneau, M., Demleitner, M., & Andrae, R. 2021, *AJ*, 161, 147
- Barman, T. S., Macintosh, B., Konopacky, Q. M., & Marois, C. 2011a, *ApJ*, 733, 65
- Barman, T. S., Macintosh, B., Konopacky, Q. M., & Marois, C. 2011b, *ApJL*, 735, L39
- Barrado y Navascués, D. 2006, *A&A*, 459, 511
- Beiler, S. A., Allers, K. N., Cushing, M., et al. 2023, *MNRAS*, 518, 4870
- Bell, C. P. M., Mamajek, E. E., & Naylor, T. 2015, *MNRAS*, 454, 593
- Betti, S. K., Follette, K. B., Ward-Duong, K., et al. 2022, *ApJ*, 935, L18
- Biller, B. A., & Close, L. M. 2007, *ApJL*, 669, L41
- Binks, A. S., & Jeffries, R. D. 2016, *MNRAS*, 455, 3345
- Böker, T., Arribas, S., Lützgendorf, N., et al. 2022, *A&A*, 661, A82
- Böker, T., Beck, T. L., Birkmann, S. M., et al. 2023, *PASP*, 135, 038001
- Bonnefoy, M., Chauvin, G., Lagrange, A.-M., et al. 2014, *A&A*, 562, A127
- Bowler, B. P., Liu, M. C., Dupuy, T. J., & Cushing, M. C. 2010, *ApJ*, 723, 850
- Bowler, B. P., Liu, M. C., Kraus, A. L., Mann, A. W., & Ireland, M. J. 2011, *ApJ*, 743, 148
- Bowler, B. P., Zhou, Y., Morley, C. V., et al. 2020, *ApJL*, 893, L30
- Burgasser, A. J., Marley, M. S., Ackerman, A. S., et al. *ApJL*, 571, L151
- Burrows, A., Marley, M., Hubbard, W. B., et al. 1997, *ApJ*, 491, 856
- Chabrier, G., Baraffe, I., Phillips, M., & Debras, F. 2023, *A&A*, 671, A119
- Charnay, B., Bézard, B., Baudino, J.-L., et al. 2018, *ApJ*, 854, 172
- Chauvin, G., Lagrange, A.-M., Dumas, C., et al. 2004, *A&A*, 425, L29
- Chauvin, G., Lagrange, A.-M., Dumas, C., et al. 2005, *A&A*, 438, L25
- Chinchilla, P., Béjar, V. J. S., Lodieu, N., Zapatero Osorio, M. R. & Gauza, B. 2021, *A&A*, 645, A17
- Cruz, K. L., Kirkpatrick, J. D., & Burgasser, A. J. 2009, *AJ*, 137, 3345
- Cruz, K. L., Núñez, A., Burgasser, A. J., et al. 2018, *AJ*, 155, 34
- Currie, T., Burrows, A., Itoh, Y., et al. 2011, *ApJ*, 729, 128
- Currie, T., Lawson, K., Schneider, G., et al. 2022, *Nature Astronomy*, 6, 751
- Cutri, R. M., Mainzer, A., Conrow, T., et al. 2023, *NEOWISE-R Single Exposure Source Table*, IPAC, doi:10.26131/IRSA144
- de la Reza, R., Torres, C. A. O., Quast, G., Castilho, B. V., & Vieira, G. L. 1989, *ApJL*, 343, L61
- Delorme, P., Gagné, J., Girard, J. H., et al. 2013, *A&A*, 553, L5
- Ducourant, C., Teixeira, R., Chauvin, G., et al. 2008, *A&A*, 477, L1
- Dupuy, T. J., Liu, M. C., Evans, E. L., et al. 2023, *MNRAS*, 519, 1688
- Edwards, S., Fischer, W., Hillenbrand, L., & Kwan, J. 2006, *ApJ*, 646, 319
- Eisenhauer, F., Abuter, R., Bickert, K., et al. 2003, *SPIE*, 4841, 1548
- Erkal, J., Manara, C. F., Schneider, P. C., et al. 2022, *A&A*, 666, A188
- Eriksson, S. C., Asensio Torres, R., Janson, M., et al. 2020, *A&A*, 638, L6
- Faherty, J. K., Burgasser, A. J., Walter, F. M., et al. 2012, *ApJ*, 752, 56
- Faherty, J. K., Riedel, A. R., Cruz, K. L., et al. 2016, *ApJS*, 225, 10
- Filippazzo, J. C., Rice, E. L., Faherty, J., et al. 2015, *ApJ*, 810, 158
- France, K., Linsky, J. L., Brown, A., et al. 2010, *ApJ*, 715, 596
- Gagné, J., Faherty, J. K., Mamajek, E. E., et al. 2017, *ApJS*, 228, 18
- Gaia Collaboration, Brown, A. G. A., Vallenari, A., Prusti, T., et al. 2021, *A&A*, 649, A1
- Gaia Collaboration, Prusti, T., de Bruijne, J. H. J., et al. 2016, *A&A*, 595, A1
- Gaia Collaboration, Vallenari, A., Brown, A. G. A., et al. 2022, *arXiv:2208.00211*
- Gardner, J. P., Mather, J. C., Abbott, R., et al. 2023, *PASP*, in press
- Gauza, B., Béjar, V. J. S., Pérez-Garrido, A., et al. 2015, *ApJ*, 804, 96
- Gizis, J. E. 2002, *ApJ*, 575, 484
- Gizis, J. E., Jao, W.-C., Subasavage, J. P., & Henry, T. J. 2007, *ApJ*, 669, L45

- Gizis, J. E., Shipman, H. L., & Harvin, J. A. 2005, *ApJ*, 630, L89
- Golimowski, D. A., Leggett, S. K., Marley, M. S., et al. 2004, *AJ*, 127, 3516
- Gregorio-Hetem, J., Lépine, J. R. D., Quast, G. R., Torres, C. A. O., & de la Reza, R. 1992, *AJ*, 103, 549
- Gullbring, E., Hartmann, L., Briceño, C., & Calvet, N. 1998, *ApJ*, 492, 323
- Haffert, S. Y., Bohn, A. J., de Boer, J., et al. 2019, *Nature Astronomy*, 3, 749
- Hartmann, L., Herczeg, G., & Calvet, N. 2016, *ARA&A*, 54, 135
- Harvey, P. M., Henning, T., Ménard, F., et al. 2012, *ApJ*, 744, L1
- Herczeg, G. J., Cruz, K. L., & Hillenbrand, L. A. 2009, *ApJ*, 696, 1589
- Herczeg, G. J., & Hillenbrand, L. A. 2008, *ApJ*, 681, 594
- Herczeg, G. J., & Hillenbrand, L. A. 2014, *ApJ*, 786, 97
- Hinkley, S., Carter, A. L., Ray, S., et al. 2022, *PASP*, 134, 095003
- Howard, A., Marcy, G. W., Johnson, J. A., et al. 2010, *Science*, 330, 653
- Jakobsen, P., Ferruit, P., Alves de Oliveira, C., et al. 2022, *A&A*, 661, A80
- Kastner, J. H., Zuckerman, B., Weintraub, D. A., & Forveille, T. 1997, *Science*, 277, 67
- Kirkpatrick, J. D., Gelino, C. R., Faherty, J. K., et al. 2021, *ApJS*, 253, 7
- Lachapelle, F.-R., Lafrenière, D., Gagné, J., et al. 2015, *ApJ*, 802, 61
- Lecavelier des Etangs, A., & Lissauer, J. J. 2022, *NewAR*, 94, 101641
- Liu, M. C., Dupuy, T. J., & Allers, K. N. 2016, *ApJ*, 833, 96
- Liu, M. C., Magnier, E. A., Deacon, N. R., et al. 2013, *ApJL*, 777, L20
- Lodato, G., Delgado-Donate, E., & Clarke, C. J. 2005, *MNRAS*, 364, L91
- Looper, D. L., Burgasser, A. J., Kirkpatrick, J. D., & Swift, B. J. 2007, *ApJL*, 669, L97
- Luhman, K. L. 2023, *AJ*, in press
- Luhman, K. L., & Esplin, T. L. 2020, *AJ*, 160, 44
- Luhman, K. L., & Esplin, T. L. 2022, *AJ*, 163, 26
- Luhman, K. L., Mamajek, E. E., Shukla, S. J., & Loutrel, N. P. 2017, *AJ*, 153, 46
- Luhman, K. L., Patten, B. M., Marengo, M., et al. 2007, *ApJ*, 654, 570
- Madhusudhan, N., Burrows, A., & Currie, T. 2011, *ApJ*, 737, 34
- Mainzer, A., Bauer, J., Cutri, R. M., et al. 2014, *ApJ*, 792, 30
- Mamajek, E. E. 2005, *ApJ*, 634, 1385
- Mamajek, E. E., & Meyer, M. R. 2007, *ApJL*, 668, L175
- Marley, M. S., Saumon, D., Cushing, M., et al. 2012, *ApJ*, 754, 135
- McMahon, R. G., Banerji, M., Gonzalez, E., et al. 2013, *The Messenger*, 154, 35
- Metchev, S. A., & Hillenbrand, L. A. 2006, *ApJ*, 651, 1166
- Metchev, S. A., Marois, C., & Zuckerman, b. 2009, *ApJL*, 705, L204
- Miles, B. E., Biller, B. A., Patapis, P., et al. 2023, *ApJL*, 946, L6
- Miles, B. E., Skemer, A. J., Barman, T. S., Allers, K. N., & Stone, J. M. 2018, *ApJ*, 869, 18
- Milli, J., Hibon, P., Christiaens, V., et al. 2017, *A&A*, 597, L2
- Mohanty, S., Greaves, J., Mortlock, D., et al. 2013, *ApJ*, 773, 168
- Mohanty, S., Jayawardhana, R., & Barrado y Navascués, D. 2003, *ApJL*, 593, L109
- Mohanty, S., Jayawardhana, R., Huélamo, N., & Mamajek, E. 2007, *ApJ*, 657, 1064
- Morrow, A. L., Luhman, K. L., Espaillat, C., et al. 2008, *ApJL*, 676, L143
- Mukherjee, S., Fortney, J. J., Batalha, N. E., et al. 2022, *ApJ*, 938, 107
- Muzerolle, J., Luhman, K. L., Briceño, C., Hartmann, L., & Calvet, N. 2005, *ApJ*, 625, 906
- Natta, A., Testi, L., Muzerolle, J., et al. 2004, *A&A*, 424, 603
- Patience, J., King, R. R., De Rosa, R. J., & Marois, C. 2010, *A&A*, 517, A76
- Patience, J., King, R. R., De Rosa, R. J., et al. 2012, *A&A*, 540, A85
- Petrus, S., Chauvin, G., Bonnefoy, M., et al. 2023, *A&A*, 670, L9
- Rayner, J. T., Toomey, D. W., Onaka, P. M., et al. 2003, *PASP*, 115, 362
- Riaz, B., & Gizis, J. E. 2008, *ApJ*, 681, 1584
- Riaz, B., Gizis, J. E., & Hmiel, A. 2006, *ApJ*, 639, L79
- Ricci, L., Cazzoletti, P., Czekala, I., et al. 2017, *AJ*, 154, 24
- Rice, E. L., Barman, T., Mclean, I., Prato, L., & Kirkpatrick, J. D. 2010, *ApJS*, 186, 63
- Rieke, G. H., Wright, G. S., Böker, T., et al. 2015, *PASP*, 127, 584
- Rieke, M. J., Kelly, D. M., & Horner, S. 2005, *SPIE*, 5904, 590401
- Rieke, M. J., Kelly, D. M., Misselt, K., et al. 2023, *PASP*, 135, 028001
- Ringqvist, S. C., Viswanath, G., Aoyama, Y., et al. 2023, *A&A*, 669, L12

- Schneider, A. C., Burgasser, A. J., Bruursema, J., et al. 2023, *ApJL*, 943, L16
- Schneider, A. C., Melis, C., & Song, I. 2012, *ApJ*, 754, 39
- Scholz, A., Jayawardhana, R., & Brandeker, A. 2005a, *ApJ*, 629, L41
- Scholz, R.-D., McCaughrean, M. J., Zinnecker, H., & Lodieu, N. 2005b, *A&A*, 430, L49
- Skemer, A. J., Close, L. M., Szűcs, L., et al. 2011, *ApJ*, 732, 107
- Skemer, A. J., Marley, M. S., Hinz, P. M., et al. 2014, *ApJ*, 792, 17
- Skrutskie, M., Cutri, R. M., Stiening, R., et al. 2003, 2MASS All-Sky Point Source Catalog, IPAC, doi:10.26131/IRSA2
- Skrutskie, M., Cutri, R. M., Stiening, R., et al. 2006, *AJ*, 131, 1163
- Song, I., Schneider, G., Zuckerman, B., et al. 2006, *ApJ*, 652, 724
- Stelzer, B., Scholz, A., & Jayawardhana, R. 2007, *ApJ*, 671, 842
- Sterzik, M. F., Pascucci, I., Apai, D., van der Blik, N., & Dullemond, C. P. 2004, *A&A*, 427, 245
- Thanathibodee, T., Calvet, N., Hernández, J., Maucó, K., & Briceño, C. 2022, *AJ*, 163, 74
- Tokunaga, A. T., Simons, D. A., & Vacca, W. D. 2002, *PASP*, 114, 180
- Tremblin, P., Amundsen, D. S., Chabrier, G., et al. 2016, *ApJL*, 817, L19
- Tremblin, P., Amundsen, D. S., Mourier, P., et al. 2015, *ApJL*, 804, L17
- Tremblin, P., Chabrier, G., Baraffe, I., et al. 2017, *ApJ*, 850, 46
- Tremblin, P., Padiou, T., Phillips, M. W., et al. 2019, *ApJ*, 876, 144
- Venuti, L., Stelzer, B., Alcalá, J. M., et al. 2019, *A&A*, 632, A46
- Wagner, K., Follette, K. B., Close, L. M., et al. 2018, *ApJL*, 863, L8
- Webb, R. A., Zuckerman, B., Platais, I., et al. 1999, *ApJL*, 512, L63
- Whelan, E. T., Ray, T. P., Comeron, F., Bacciotti, F., & Kavanagh, P. J. 2012, *ApJ*, 761, 120
- Whelan, E. T., Ray, T. P., Randich, S., et al. 2007, *ApJL*, 659, L45
- Wright, E. L., Eisenhardt, P. R., Mainzer, A. K., et al. 2010, *AJ*, 140, 1868
- Wright, E. L., Eisenhardt, P. R. M., Mainzer, A. K., et al. 2013, AllWISE Source Catalog, IPAC, doi:10.26131/IRSA134
- Zhou, Y., Bowler, B. P., Apai, D., et al. 2022a, *AJ*, 164, 239
- Zhou, Y., Bowler, B. P., Morley, C. V., et al. 2020, *AJ*, 160, 77
- Zhou, Y., Bowler, B. P., Wagner, K. R., et al. 2021, *AJ*, 161, 244
- Zhou, Y., Herczeg, G. J., Kraus, A. L., Metchev, S., & Cruz, K. L. 2014, *ApJL*, 783, L17
- Zhou, Y., Sanghi, A., Bowler, B. P., et al. 2022b, *ApJL*, 934, L13

Table 1. Synthetic NIRSpect Photometry for TWA 27A/B, TWA 28, and VHS 1256b

Column Label	Description
Name	Source name
Jmag	<i>J</i> 2MASS magnitude
Hmag	<i>H</i> 2MASS magnitude
Ksmag	<i>K_s</i> 2MASS magnitude
Jmkomag	<i>J</i> MKO magnitude
Hmkomag	<i>H</i> MKO magnitude
Kmkomag	<i>K</i> MKO magnitude
W1mag	W1 WISE magnitude
W2mag	W2 WISE magnitude
m115mag	F115W NIRCcam magnitude
m140mag	F140M NIRCcam magnitude
m150mag	F150W NIRCcam magnitude
m162mag	F162M NIRCcam magnitude
m182mag	F182M NIRCcam magnitude
m200mag	F200W NIRCcam magnitude
m210mag	F210M NIRCcam magnitude
m250mag	F250M NIRCcam magnitude
m277mag	F277W NIRCcam magnitude
m300mag	F300M NIRCcam magnitude
m335mag	F335M NIRCcam magnitude
m356mag	F356W NIRCcam magnitude
m360mag	F360M NIRCcam magnitude
m410mag	F410M NIRCcam magnitude
m430mag	F430M NIRCcam magnitude
m444mag	F444W NIRCcam magnitude
m460mag	F460M NIRCcam magnitude
m480mag	F480M NIRCcam magnitude

NOTE— The table is available in its entirety in machine-readable form.

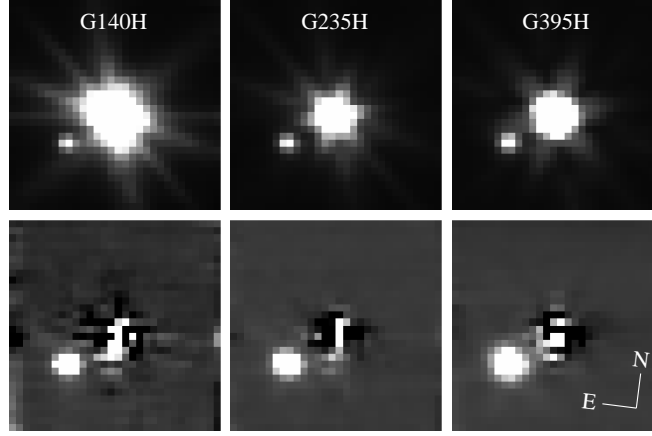


Figure 1. NIRSpect IFU images of TWA 27A and B after collapsing along the dispersion direction, before and after PSF subtraction of the primary (top and bottom). The size of each image is $3'' \times 3''$.

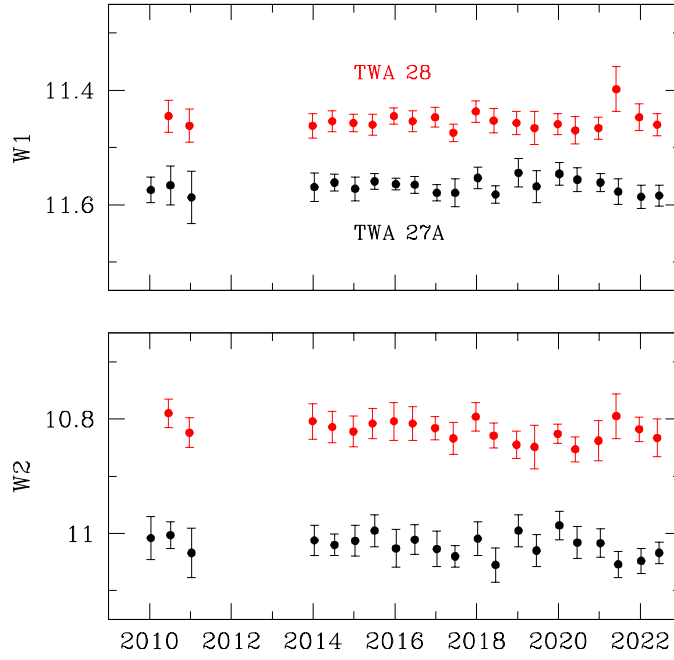


Figure 2. Medians and standard deviations of WISE/NEOWISE data for TWA 27A and TWA 28 among the single exposures taken during epochs spanning ~ 1 –4 days.

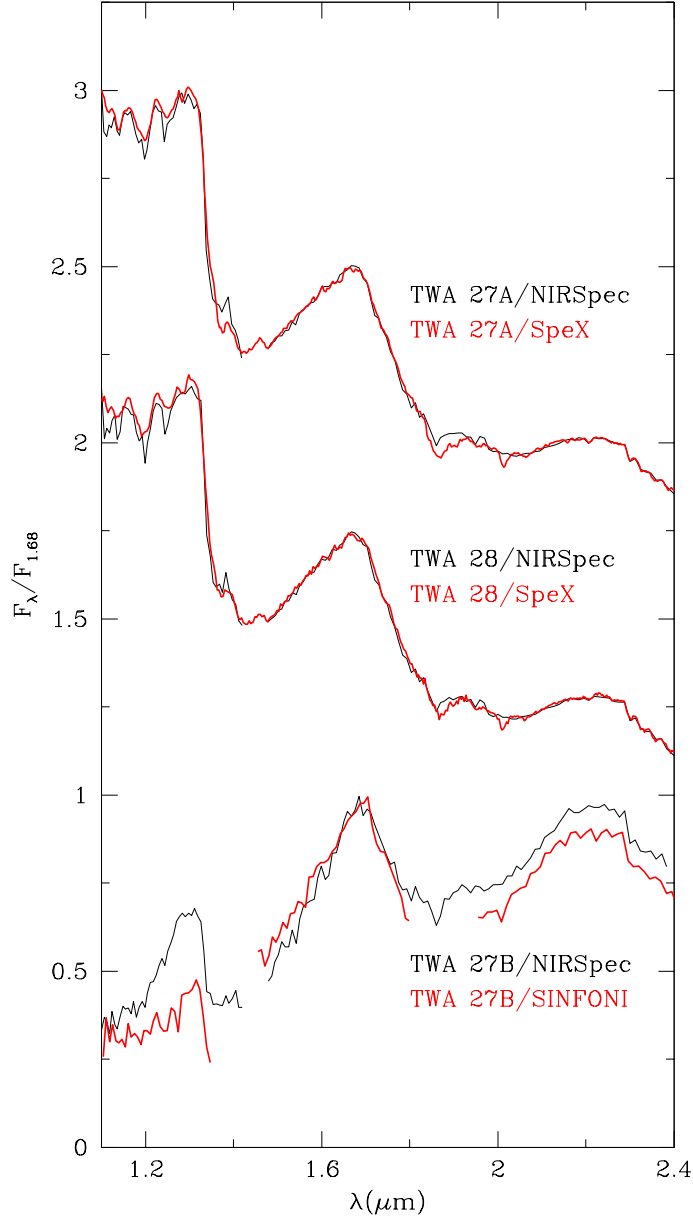


Figure 3. Comparison of near-IR spectra from NIRSpec (this work) and ground-based instruments (Looper et al. 2007; Patience et al. 2010; Luhman et al. 2017). The NIRSpec and SINFONI data have been binned to a resolution of $R=200$. The relative flux calibrations of the J and HK spectra from SINFONI were based on uncertain photometry in J and K .

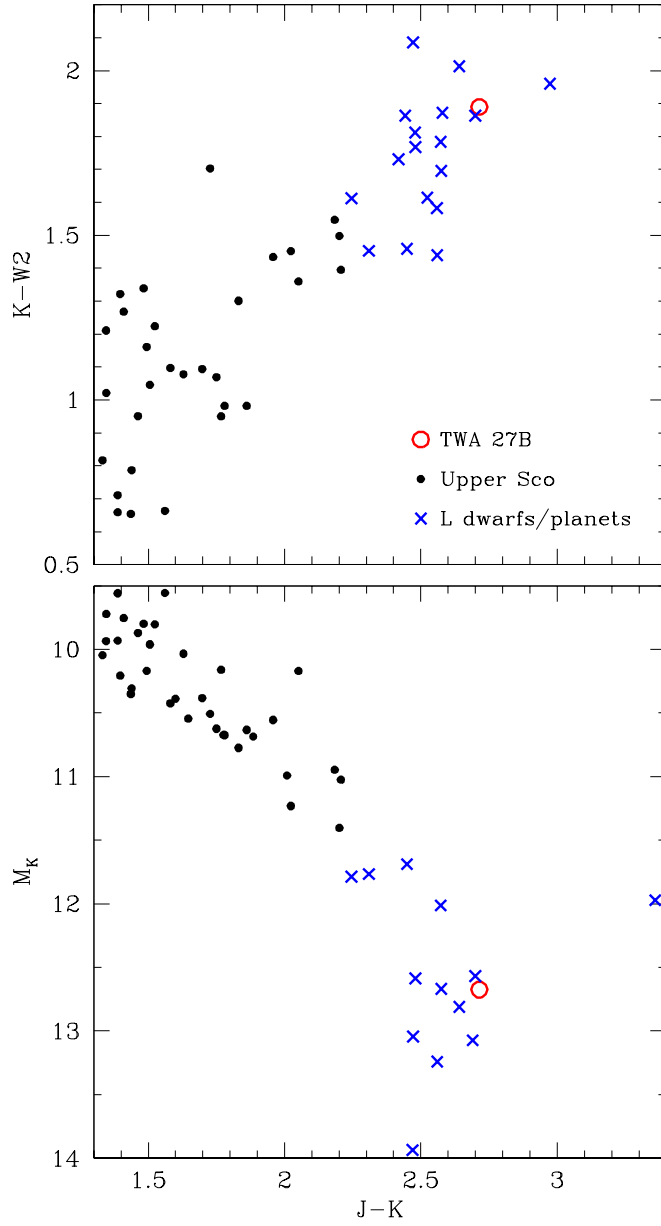


Figure 4. $K-W2$ and M_K versus $J-K$ for TWA 27B, members of Upper Sco (Luhman & Esplin 2022, K. Luhman, in preparation), and red L-type dwarfs and planets (Schneider et al. 2023, references therein). Some of the L-type objects appear in only one diagram because they lack parallax measurements or W2 photometry.

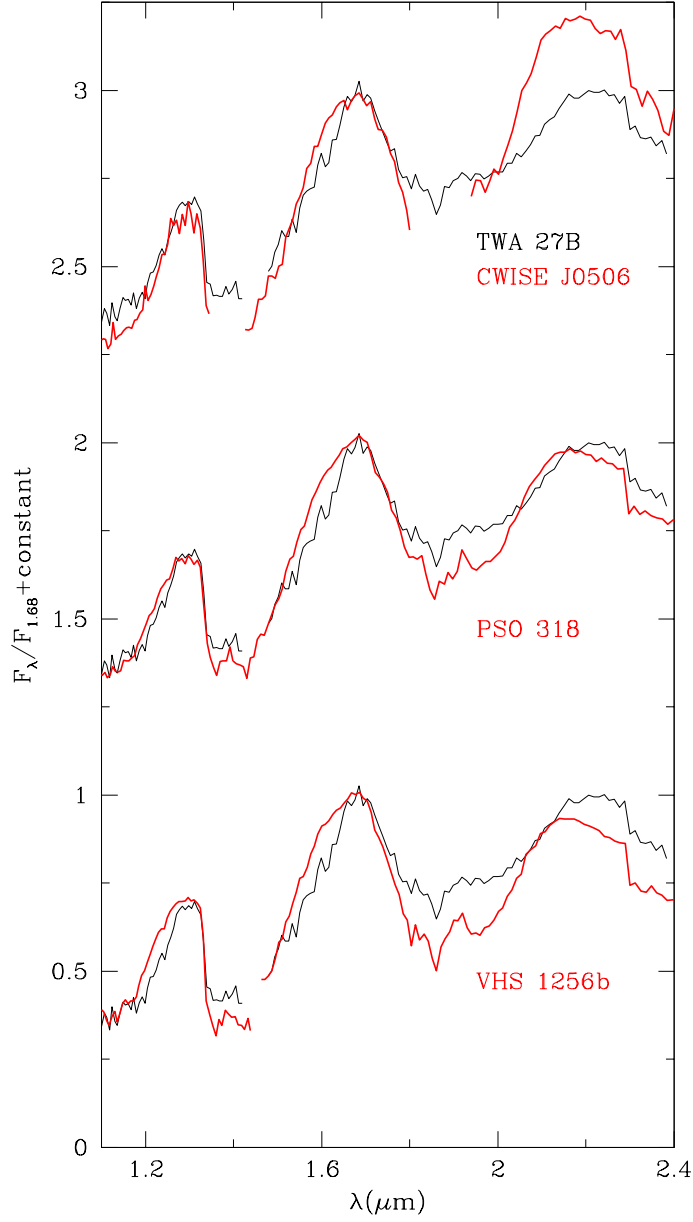


Figure 5. Near-IR spectrum of TWA 27B from JWST/NIRSpec (this work) compared to spectra of CWISE J0506 (Schneider et al. 2023), PSO 318 (Liu et al. 2013), and VHS 1256b (this work; see also Miles et al. (2023)). The spectra have been binned to a resolution of $R=200$.

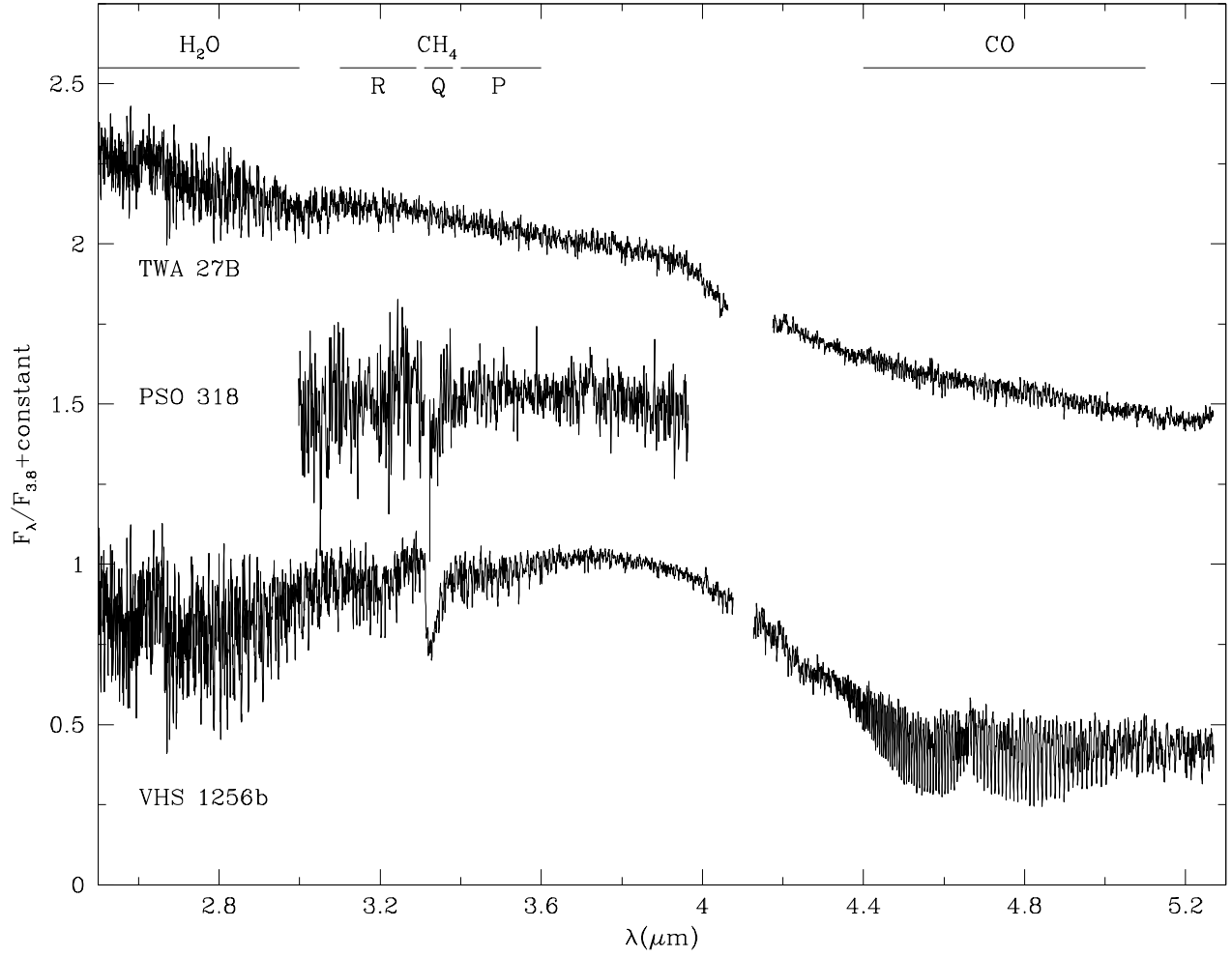


Figure 6. Mid-IR spectra of TWA 27B (this work), PSO 318 (Beiler et al. 2023), and VHS 1256b (this work; see also Miles et al. (2023)).

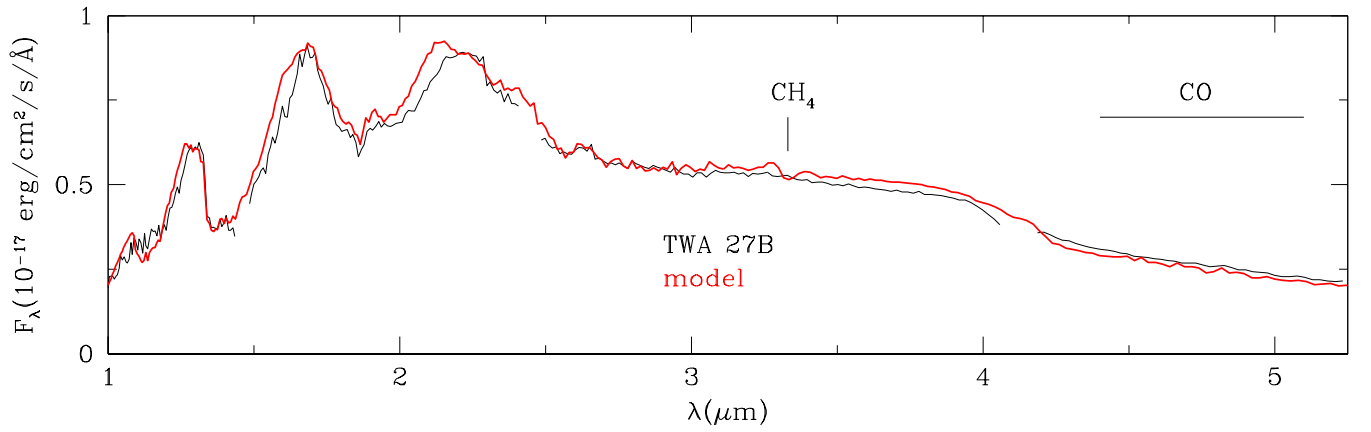


Figure 7. IR spectrum of TWA 27B from JWST/NIRSpec compared to a model spectrum for a cloudless atmosphere with $T_{\text{eff}} = 1300$ K, $\log g = 3.5$, $\gamma = 1.03$, $K_{\text{zz}} = 10^5$, $[\text{M}/\text{H}] = 0.2$, a solar value for C/O, and $R = 0.116 R_{\odot}$ (Tremblin et al. 2017; Petrus et al. 2023). The spectra have been binned to a resolution of $R=200$.

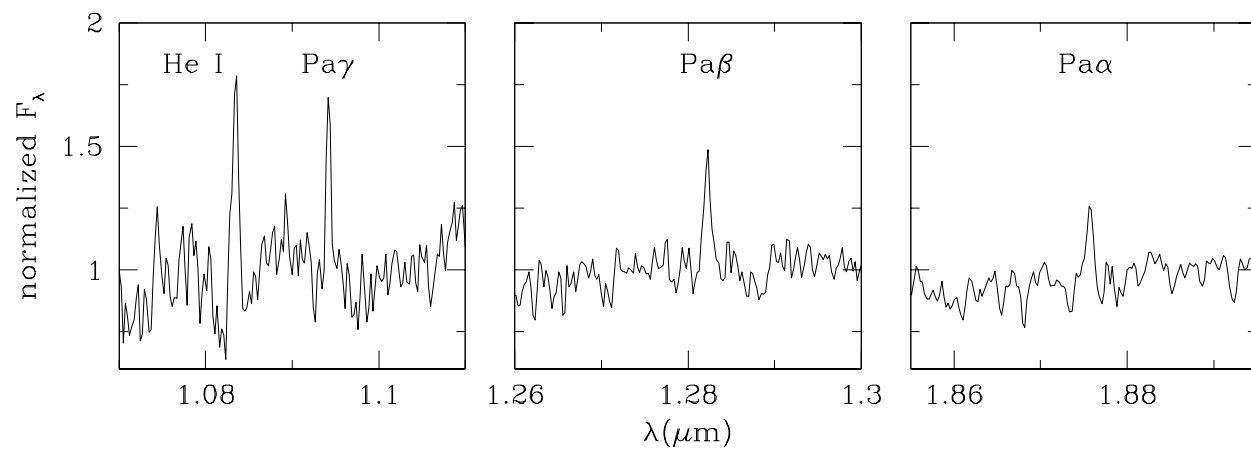


Figure 8. Detections of He I and Paschen emission lines in the JWST/NIRSpec spectrum of TWA 27B.

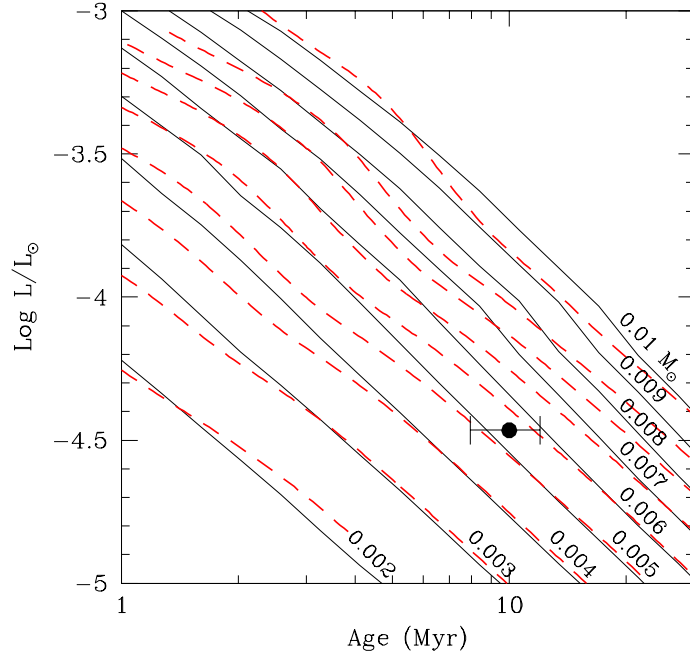


Figure 9. Luminosity estimate for TWA 27B compared to luminosities as a function of age predicted by evolutionary models of [Chabrier et al. \(2023\)](#) (solid lines) and [Burrows et al. \(1997\)](#) (dashed lines).